IRSTI 31; 31:17; 31:17:15 https://doi.org/10.26577/IJBCh2023v16i2a12

G. Burashev[1], B. Tatykayev[1], M. Baláž[2], N. Khan[1], A. Seysembekova[1], S. Tugelbay[1], N. Turgynbay[1], M. Burkitbayev[1], Zh. Shalabayev[1*]

[1]Al-Farabi Kazakh National University, Almaty, Kazakhstan
[2]Institute of Geotechnics, Slovak Academy of Sciences, Košice, Slovakia
*e-mail: zhandos.shalabay@gmail.com
(Received 16 October 2023; received in revised form 13 November 2023;accepted 03 December 2023)

All solid-state fabrication strategy of CdS@ZnS nanocomposites and their photocatalytic performance in water purification

Abstract. Herein a systematic study of two-step solid-phase synthesis of CdS@ZnS nanocomposites and their photocatalytic activity is presented. First, CdS nanoparticles were synthesized in a planetary ball mill through a solid-state ion exchange reaction. In the second step, Cd^{2+} ions were partially replaced by Zn^{2+} ions at the surface of the nanoparticles using solvent free long-term activation in a high-energy planetary ball mill. The optimal activation time in a ball mill was determined to be 45 min. Spherical CdS nanoparticles with a diameter of 10 nm and modified CdS@ZnS (45 min) nanocomposites were characterized by X-ray diffraction analysis, Raman and UV-vis spectroscopy, and scanning electron microscopy. The ability of nanocomposites for photocatalytic water purification was tested on the degradation of the model organic dye Orange II in an aqueous solution under the visible light irradiation. The modified CdS@ZnS nanocomposites showed higher photocatalytic activity compared to the original CdS nanoparticles.
Key words: solid-state synthesis; mechanochemistry; cadmium sulfide; zinc sulfide; photocatalysis; hydrogen evolution.

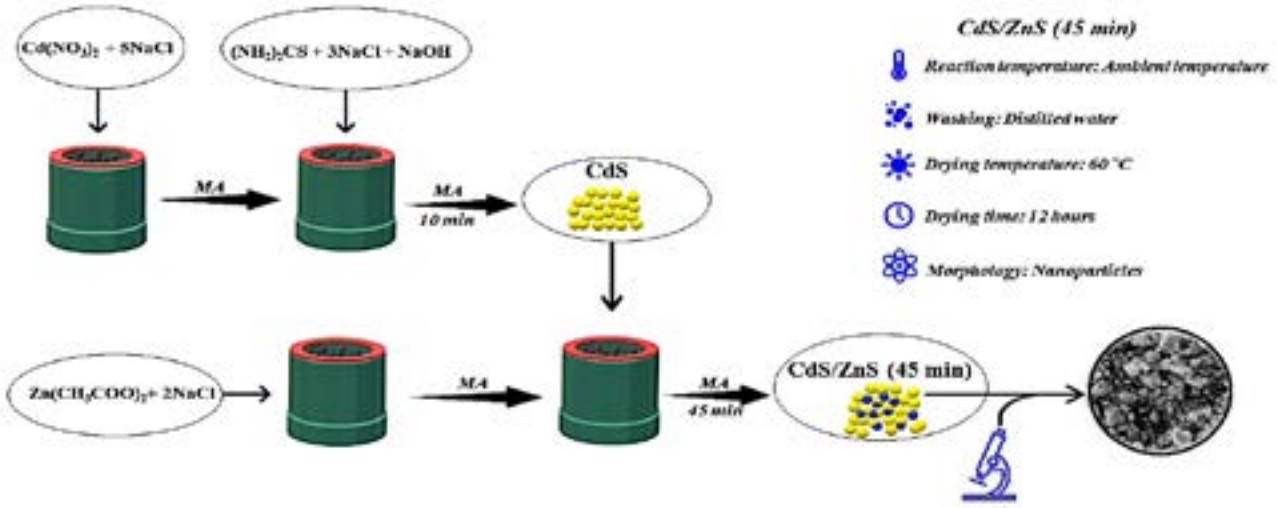

Introduction

Wastewater pollution poses a significant environmental and public health challenge globally [1]. Various human activities, including industrial processes, agriculture, and domestic sewage, contribute to the discharge of wastewater containing a range of contaminants into water. These contaminants include organic and inorganic pollutants, nutrients, heavy metals, and pathogens [2].

Photocatalysis has emerged as a highly effective method for wastewater treatment [3].

Semiconductor photocatalysts, such as metal sulfide nanoparticles and binary, ternary nanocomposites based on them, harness light energy to initiate photocatalytic reactions that can efficiently degrade organic pollutants and remove contaminants from wastewater [4]. The photocatalytic process involves the generation of electron-hole pairs upon light absorption, which induces redox reactions and breaks down pollutants into less harmful byproducts. Semiconductor photocatalysts offer advantages such as high efficiency, versatility, and the ability to operate under ambient conditions [5, 6].

Nanocomposites based on CdS nanoparticles and their composites with other semiconducters have been recommended as strong photocatalysts in water purification and hydrogen production [7]. Their ability to absorb visible light enables efficient degradation of organic pollutants and removal of harmful substances from water. Additionally, these nanoparticles exhibit remarkable performance in photocatalytic water splitting, facilitating the production of clean and sustainable hydrogen gas. CdS@ZnS nanoparticles offer promising solutions for addressing water pollution and advancing renewable energy technologies.

Also, CdS@ZnS nanocomposites find applications in diverse fields such as solar cells and photovoltaics [8], optoelectronics and light-emitting diodes [9], as well as sensing and biosensing [10]. Their unique properties enable enhanced light absorption, improved charge transport, and efficient photocatalytic activity, making them promising materials for next-generation energy devices, environmental remediation technologies, and advanced sensing platforms [11].

There are many preparation methods of CdS@ ZnS nanocomposites such as aqueous synthesis [12], reverse micellar [13], microjet reactor technology [14], *in situ* synthesis [15], hydrothermal [16], chemical [11], microwave-assisted synthesis [17], electrosynthesis [18], microemulsion technique [19], and mechanochemical approach [20, 21].

The last one is of particular interest because mechanochemistry, the process of using mechanical force to initiate chemical reactions, offers several advantages in the field of chemistry [22]. Firstly, it enables reactions to occur without the need of using of toxic chemicals as precursors and high temperatures, making it environmentally friendly and energy-efficient. Secondly, mechanochemistry often leads to higher yields and purer products compared to traditional methods, reducing waste and improving overall efficiency [23]. Additionally, it allows the synthesis of compounds that might be challenging to produce using conventional methods, expanding the scope of possible materials and innovations in various industries [24].

In this work, the surface of mechanochemically synthesized CdS nanoparticles was coated with ZnS. CdS nanoparticles were co-milled with zinc acetate in a high-energy planetary ball mill for a long time. According to our strategy, Cd^{2+} ions from the surface CdS nanoparticles were replaced by Zn^{2+} ones. As a result, CdS@ZnS with high photocatalytic activity was obtained.

Materials and methods

Materials. Cadmium nitrate tetrahydrate ($Cd(NO_3)_2 \cdot 4H_2O$, Sigma-Aldrich, Taufkirchen, Germany), thiourea ($CS(NH_2)_2$, Sigma-Aldrich, Taufkirchen, Germany), sodium hydroxide (NaOH, Sigma-Aldrich, Taufkirchen, Germany), sodium chloride(NaCl,Sigma-Aldrich,Taufkirchen,Germany), zinc acetate dihydrate ($Zn(CH_3COO)_2 \cdot 2H_2O$, Sigma-Aldrich, Taufkirchen, Germany), and Orange II sodium salt ($C_{16}H_{11}N_2NaO_4S$, Sigma-Aldrich, Taufkirchen, Germany) were of analytical grade and used without further purification.

Characterization. X-ray diffraction patterns were obtained on a MiniFlex 600 diffractometer (Rigaku, Japan) in a digital form using copper radiation. Sample analysis modes were as follows: X-ray tube voltage – 40 kV, the tube current – 15 mA, goniometer movement step size – 0.02 °, and step time 0.12 sec. During shooting, the sample was rotated in its plane at a speed of 60 rpm. For phase analysis, the ICCD-PDF2 Release 2016 database and the PDXL2 software have been used.

The study of optical phonon modes was carried out via Raman spectroscopy on a LabRAM HR Evolution spectrometer, Horiba Scientific (Japan), in the range of 100-2000 cm^{-1} (acquisition time – 15 seconds, accumulation – 3) and a laser with a wavelength of 532 nm (objective – 10X, hole – 300).

A UV-2600i compact UV spectrophotometer was used to evaluate the absorption spectra in the UV-visible region to determine the band gap energy of semiconductors.

The morphology and size of the prepared samples were investigated utilizing scanning electron microscopy (SEM). SEM images were obtained with the help of a scanning electron microscope ZEISS Crossbeam 540.

Mechanochemical synthesis of CdS/ZnS nanocomposites. The synthesis process of the ZnS

doped CdS NPs (CdS/ZnS) involved two primary stages.

In the first stage, 0.8181 g of dehydrated $Cd(NO_3)_2$ was used and activated alongside 1.0111 g of NaCl, which served as a diluent. Another component, $(NH_2)_2CS$ 0.2634 g, underwent similar activation with 0.6067 g of NaCl to create a homogeneous mixture. Subsequently, all reactants were placed in a ball mill for mechanochemical synthesis. The experiment was conducted in the presence of 0.1384 g of NaOH. The resulting CdS product was subjected to multiple washes with bidistilled water to eliminate unwanted by-products. Subsequently, the CdS nanoparticles were dried for 12 hours at 60 °C.

In the subsequent stage, 0.6350 g of $Zn(CH_3COO)_2$ was also activated in the presence of 0.4045 g of NaCl. The activated product was combined with the pre-dried CdS from the first stage for mechanical activation, yielding the CdS/ZnS composite. The resulting product underwent a similar series of washes with bidistilled water and was then dried at 60 °C for approximately 12 hours.

The mechanochemical experiments were conducted within the Activator 2SL ball mill (Activator, Russia). The specific experimental conditions were as follows: the rotational speed was maintained at 400 rpm, and the ball-to-powder ratio was set to 37, employing 10 mm diameter silicon nitride balls, with a total of 20 balls utilized. The grinding chamber's volume was 100 mL, made from silicon nitride (Si_3N_4), and the milling was performed in air. The synthesis duration comprised two stages: the initial stage lasting 10 minutes and the subsequent stage 15, 30, 45 and 60 minutes.

The chemical reaction for both stages proceeded as follows:

$$Cd(NO_3)_2 + (NH_2)_2CS + 2NaOH \rightarrow CdS + 2NaNO_3 + (NH_2)_2CO + H_2O \quad (1)$$

$$2CdS + Zn(CH_3COO)_2 \rightarrow CdS + ZnS + Cd(CH_3COO)_2 \quad (2)$$

Synthesis of CdS/ZnS (45 min) doped NiS nanostructures. To investigate the photocatalytic production of hydrogen, we incorporated a co-catalyst, specifically nickel sulfide (NiS), to enhance the photocatalytic activity. Catalysts play a pivotal role in augmenting catalytic activity by efficiently collecting photoexcited electrons or holes [25]. In this study, we synthesized a NiS co-catalyst using nickel nitrate hexahydrate ($Ni(NO_3)_2 \times 6H_2O$) and sodium sulfide nonahydrate ($Na_2S \times 9H_2O$). We applied the NiS co-catalyst onto the surface of the photocatalyst during the deposition process, resulting in a composite material with approximately 1.5% NiS by weight, ensuring the presence of the requisite co-catalyst in the final material.

Photocatalytic experiments. The protocol of investigation of photocatalytic activity of the prepared nanocomposites was similar to our previous studies [26-28]. To study the photocatalytic properties of the resulting nanocomposites Orange II organic dye at a concentration of 20 mg/L was used. Specifically, 20 mg of the nanocomposite was transferred into 40 mL of an aqueous solution of Orange II. The experiments were conducted under visible light illumination using an Osram Vita Lux lamp (300 W) with a light intensity of 15 mW/cm². The lamp was positioned 20 cm above the model solution's surface, and an organic glass cut-off filter was utilized to restrict irradiation to wavelengths above 400 nm.

Before initiating light irradiation, the suspensions were stirred in the dark for 60 minutes. Every 30 minutes during this period, 2.5 mL of the suspension was taken to assess the adsorption-desorption properties between the photocatalyst and the model solution. Subsequently, light irradiation was started, and the extraction of 2.5 mL of the suspension every 30 minutes was conducted, to measure the degree of photocatalytic degradation. The absorption spectra were recorded with the help of a UV-Vis spectrophotometer (SF-56, LOMO, Russia). To ensure the accuracy of the obtained results, all photocatalytic tests were repeated two times.

The stability of the photocatalysts was studied over 5 cycles of Orange II degradation. After each cycle photocatalyst was washed with deionized water and reused in the next cycle.

Hydrogen generation. The experiment utilized a flask-shaped reactor equipped with three necks and an external light source. A xenon arc lamp with a power rating of 300 watts served as the light source. This visible light source was positioned at a distance of 20 cm from the reactor and was fitted with an ultraviolet filter with a threshold wavelength of λ = 420 nm,

restricting the range of wavelengths employed. The light irradiation intensity inside the photoreactor was maintained at 15 mW/cm².

In the photocatalytic experiment for hydrogen production from water, a CdS/ZnS composite doped with NiS was employed as the photocatalyst. For the preparation of the reaction solution, 10 mL of glycerin and 90 mL of bidistilled water were added to 30 mg of the photocatalyst. The mixture was dissolved using a magnetic stirrer to ensure uniform dispersion of the photocatalyst. To eliminate excess dissolved oxygen from the reactor, argon gas was introduced (with a purity of 99.99% by weight) through the reaction mixture. The argon bubbling process was sustained for 60 minutes at a 100 mL/min flow rate. It is important to note that during this stage, the reaction mixture was shielded from light radiation. Once the bubbling process concluded, the light source was activated, and argon continued to be supplied at a rate of 5 mL/min. Argon also functioned as a carrier for the transfer of hydrogen produced as a result of the photocatalytic reaction from the reactor to a gas chromatograph (Chromos 1000, Russia) for subsequent analysis. The reactor maintained a continuous connection with the gas chromatograph in real time for the purpose of continuous monitoring. Hydrogen concentration measurements were taken every 30 minutes following the initiation of irradiation.

Results and discussion

XRD analysis. X-ray diffraction analysis was employed to investigate the crystal structure and phase purity of the synthesized nanocomposites. The presence of multiple diffraction peaks, exhibiting a broad profile in this spectrum can be attributed to the polycrystalline nature of the synthesized CdS nanoparticles [29]. Additionally, the indistinct background in the X-ray spectrum may be attributed to amorphous characteristics resulting from the irregular arrangement of lattice elements. The observed intense diffraction peaks align perfectly with the cubic phase of cadmium sulfide (JCPDS card no. 80-0019). The broadened peaks suggest that the particle sizes are within the nanoscale range [30, 31].

Furthermore, in the subsequent figure, it is noteworthy that the X-ray diffraction pattern of CdS/ZnS reveals additional peaks at 24.5° (111), 44.5° (220), and 56.4° (311). The X-ray diffraction pattern does not exhibit peaks corresponding to the crystal planes of the standard cubic structure of ZnS. Instead, the peaks at the (111), (220), and (311) planes correspond closely to the standard cubic ZnS (JCPDS card no. 05-0492) [32]. No other phases were detected. Given the limited quantity of synthesized ZnS, it is possible that their peaks are concealed amid the CdS peaks, which strongly suggests the presence of a zinc-blende ZnS shell [33].

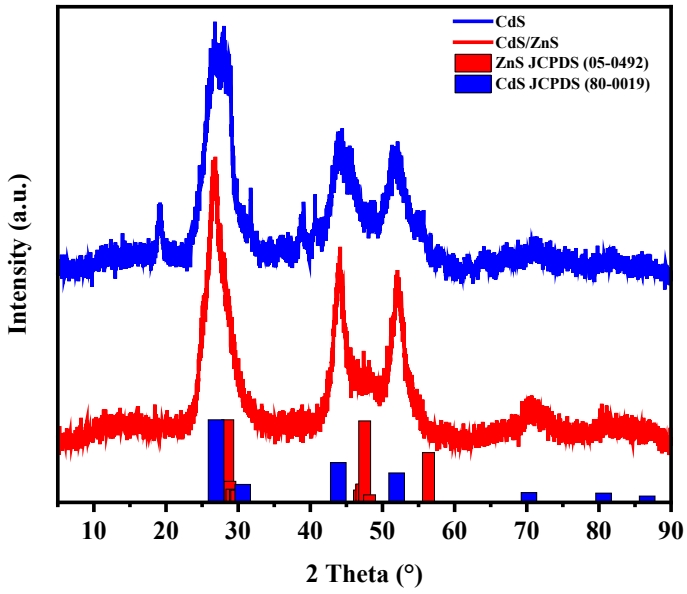

Figure 1 – XRD patterns of the a) CdS and b) CdS/ZnS nanoparticles

Raman spectroscopy. On Figure 2, the Raman spectrum of heterostructured CdS and CdS/ZnS nanocomposites is shown. For CdS and CdS/ZnS nanocrystals, three characteristic peaks were equally observed at 297.9 cm^{-1}; 598.1 cm^{-1} and 820 cm^{-1}, the corresponding second- and third-order overtones of the optical phonons 1LO, 2LO and 3LO, respectively [34]. The obtained spectra of CdS and CdS/ZnS nanocomposites are not completely different in longitudinal optical phonon modes, but the intensity of the CdS mode is somewhat sharper [35]. The optical (LO) phonon peaks of ZnS at 353 cm^{-1} may be lost between the larger peaks of CdS, which is similar to the report [36]. The observed LO Raman peak position aligns well with the reported LO phonon peak position characteristic of the cubic CdS structure. Additionally, no discernible peaks corresponding to hexagonal CdS were detected, providing indirect confirmation of the cubic zinc-blende structure in the CdS microspheres [37, 38].

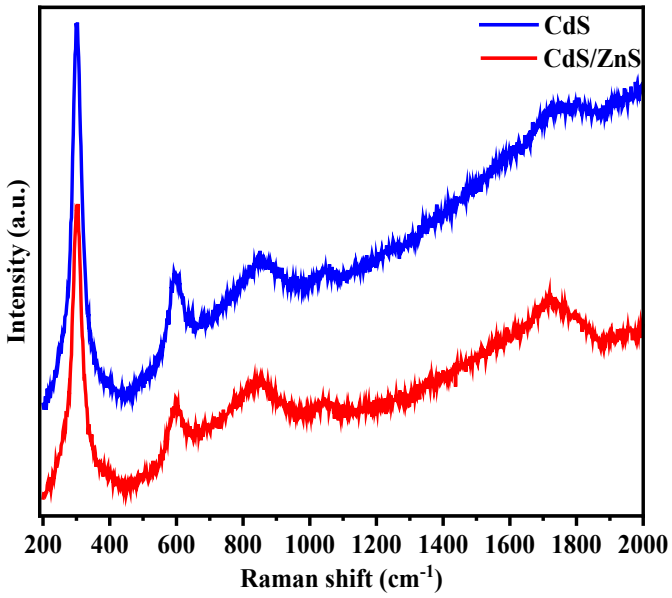

Figure 2 – Comparative Raman spectroscopy of CdS and CdS/ZnS samples employing a 532 nm laser

UV-Vis spectroscopy. Figure 3 shows the UV-Vis spectra of the mechanochemically synthesized CdS and CdS/ZnS samples. The results show that the absorption spectrum of CdS/ZnS lies higher than that of CdS. In order to find the band gaps of the synthesized samples, the Tauc plot method and the plot of $(\alpha h\gamma)^2$ versus photon energy (hv) were used. Additionally, the formula $\alpha h\nu=(h\nu-Eg)1/2$ (1) was employed, where α is the absorption coefficient, hv is the photon energy, and Eg is the direct band gap energy.

The absorption edge of CdS synthesized mechanochemically is at 565 nm (2.29 eV) [30, 39]. Compared with other CdS synthesis works, it is red shifted. It is believed that the shift in the absorption peak is obviously caused by the quantum confinement effect. The absorption edge of CdS/ZnS was at slightly lower wavelength, namely at 555 nm (2.33 eV) [40, 41].

SEM analysis. Cadmium sulfide nanoparticles have a size in range from 0.1 to 10 μm, as shown in Figure 4a. The nanoparticles are agglomerated into particles of different sizes, where the sizes range up to 10 microns. But these agglomerates are easily destroyed into individual nanoparticles when dispersed in water with ultrasonic radiation. When using nanoparticles as photocatalysts, the nanoparticle powder is dispersed in an aqueous solution. Cadmium sulfide nanoparticles were modified with zinc sulfide by solid-phase doping, and SEM images of prepared CdS/ZnS nanocomposites are presented in Figure 4b. The morphology and texture of the CdS/ZnS nanocomposites are the same as cadmium sulfide nanoparticles before modification.

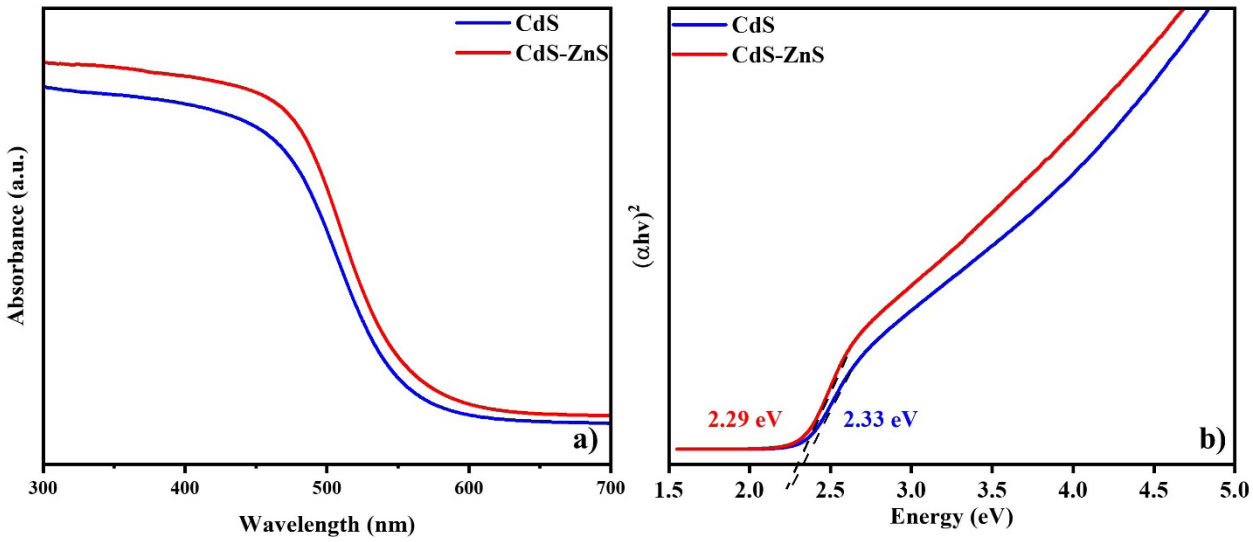

Figure 3 – (a) UV-vis absorption spectra;
(b) band gaps of CdS and CdS/ZnS estimated by $(\alpha h\upsilon)^2$ vs. photonenergy curve

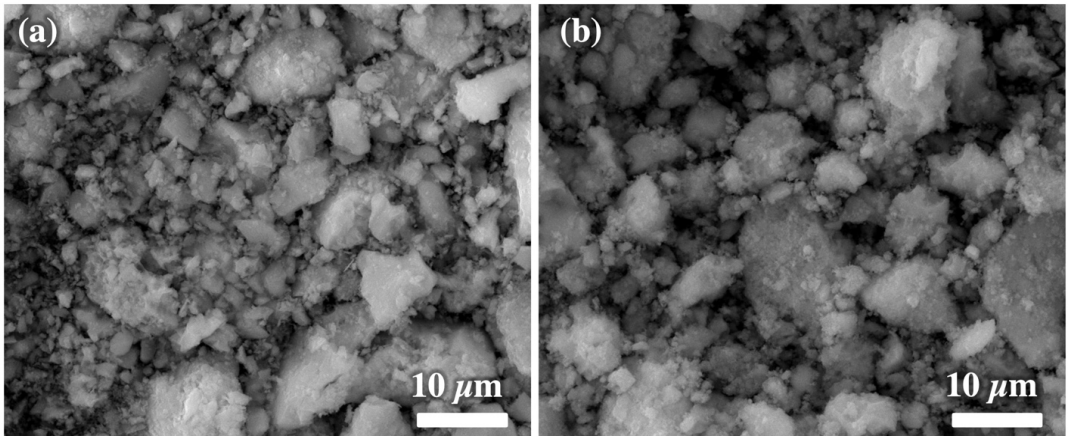

Figure 4 – SEM images of (a) CdS nanoparticles and (b) CdS/ZnS nanocomposites

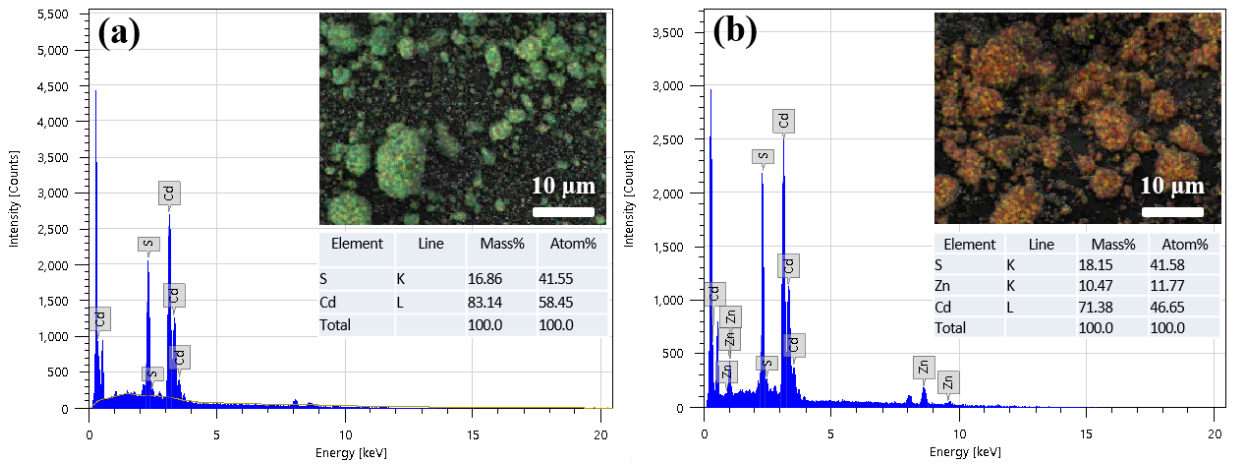

Figure 5 – SEM EDX spectrum images of (a) CdS nanoparticles and (b) CdS/ZnS nanocomposites

SEM EDX spectrum images of CdS nanoparticles and CdS/ZnS nanocomposites are presented in Figure 5. CdS nanoparticles were fabricated without contaminations. Doping with zinc sulfide occurred only on the surface of cadmium sulfide nanoparticles, and since the mass fraction of zinc in the nanocomposite according to the SEM EDX spectrum is around 10.5 %.

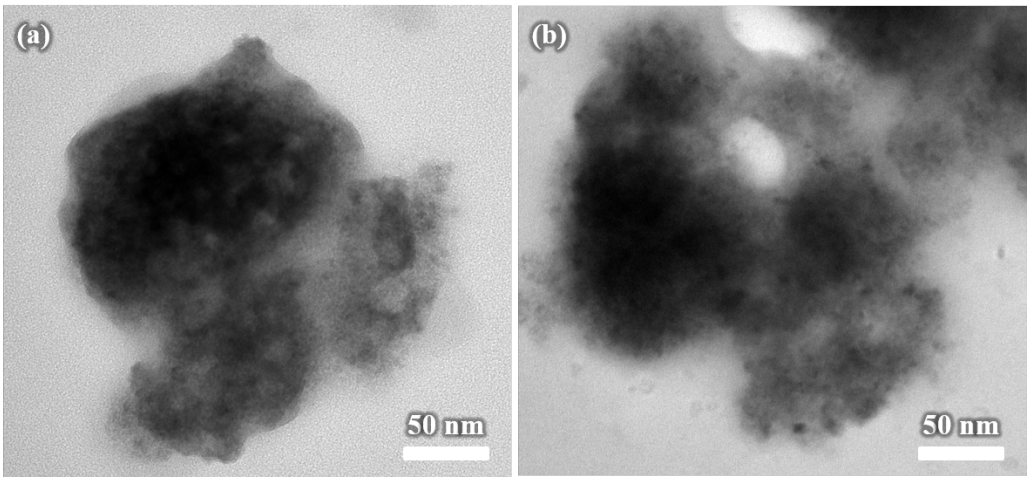

Figure 6 – TEM images of (a) CdS nanoparticles and (b) CdS/ZnS nanocomposites

TEM images are shown in Figure 6. Agglomerates of cadmium sulfide nanoparticles are actually composed of smaller particles of about 10 nm in size, as shown in Figure 6a. After doping cadmium sulfide nanoparticles with zinc ions, the morphology and size of the nanoparticles did not change, Figure 6b.

Photocatalytic activity. The results of the photocatalytic activity investigation of the composites prepared after different time are given in Figure 7a. According to the graph, after the starting of visible light irradiation, the samples immediately began to decompose the organic dye. The highest ability of Orange II degradation was demonstrated by CdS/ZnS (45 min) nanocomposite, indicating that 45 minutes of mechanochemical treatment is optimal for manifesting photocatalytic activity. It should be mentioned that the difference in the photocatalytic activity among the nanocomposites was not so big. The activity of the samples decreased from left to right as follows: CdS/ZnS (45 min), degraded about 99% molecules of Orange II → CdS/ZnS (30 min), (97%) → CdS/ZnS (15 min), (90%) → CdS/ZnS (60 min), (88%). The photocatalytic activity of the best photocatalyst, namely the CdS/ZnS (45 min) was compared with the bulk CdS (Figure 7b). As can be seen, CdS/ZnS (45 min) nanocomposite exhibits slightly worse activity.

The kinetics of the photocatalytic process was studied only for nanocomposites and depicted in Figure 7c. The order of the photocatalytic reactions was accepted as a pseudo-first-order reaction and the rate constants were found through the Langmuir–Hinshelwood kinetics model [42]:

$$ln\frac{C_0}{C} = kt \qquad (3)$$

where C_0 and C are initial concentrations of the model solution in the moment of time t and k (min^{-1}) is the rate constant of the process. The correlation coefficient R^2 served as proof of the kinetic order of decomposition of Orange II. The k and R^2 values are displayed in Table 1. Based on the data in Table 1 the k of the CdS/ZnS (45 min) is 1.34, 1.15 and 1.68 times higher than samples prepared during 15, 30 and 60 min, respectively, what indicates that CdS/ZnS (45 min) is a prospective candidate for the next study.

In addition, the cyclic tests for all nanocomposites were conducted, as the stability of the photocatalysts is one of the important properties [43]. Consequently, the results of the study (Figure 7d) demonstrate that during the first three cycles, the activity of the samples remains almost unchanged, after which there is a slight decrease in photocatalytic activity. Such results can be explained by the washing of powders from suspensions during each sampling. In general, the produced nanocomposites are relatively stable.

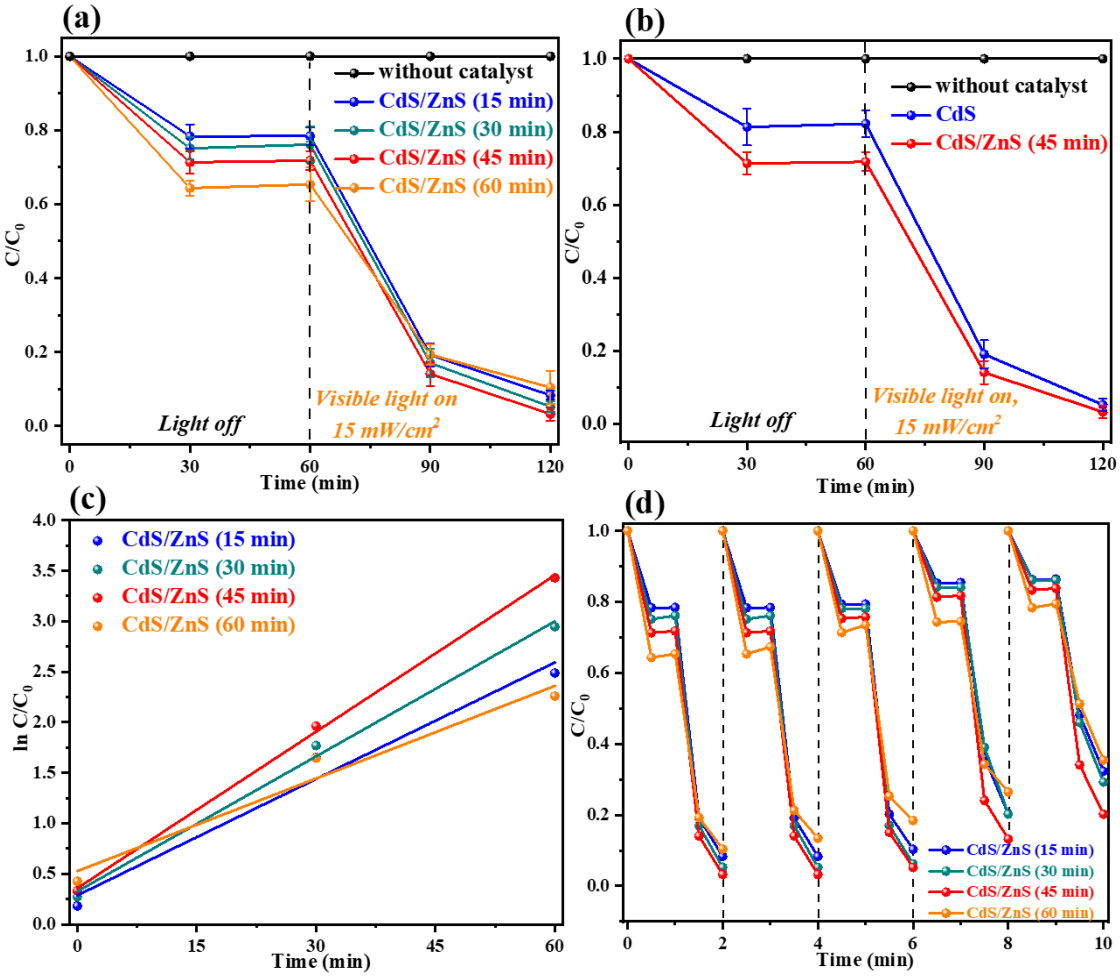

Figure 7 – a) Comparison of the photocatalytic activity of all nanocomposites; b) comparison of the photocatalytic activity of CdS/ZnS (45 min) nanocomposite and CdS, ZnS bulk materials; c) kinetic linear simulation curves for Orange II photocatalytic degradation by all nanocomposites; d) Cycling degradation efficiency of all nanocomposites

Table 1 – The k and R^2 values of the CdS/ZnS nanocomposites

The sample	k, min^{-1}	R^2
CdS/ZnS (15 min)	0.0384	0.98
CdS/ZnS (30 min)	0.0446	0.99
CdS/ZnS (45 min)	0.0516	0.99
CdS/ZnS (60 min)	0.0306	0.96

The obtained results were similar to the study [44] and the behaviour of the bulk material, CdS and ZnS nanocomposites is almost the same. However, the slight difference in activity among the nanocomposites of this study should be clarified. It is known, that mechanochemical synthesis leads to the formation of defects in the lattice of the material [45], which can play the role of the active centres that can improve the photoconductivity of electrons of semiconductors. Moreover, this method of synthesis provides the increasing of the surface area of the crystals and such systems exhibit heterogeneity [46]. Thus, the 15 and

30 minutes duration of the mechanosynthesis, seems not enough for the formation of the needed amount of active centres on the surface of CdS and ZnS, while the duration of 60 minutes leads to the rapid recombination between electrons and holes, which retard the flow of photocatalytic reactions. This is why the 45-minute duration of mechanosynthesis produced the most photocatalyticaly active material.

Analysis of the literature sources revealed that photocatalyst based on CdS and ZnS were prepared by various methods. Table 2 provides a summary of methods and conditions for producing CdS and ZnS-based materials and their photocatalytic properties, including light source, type of organic dye, efficiency and rate constants. As can be seen from the data, the most time-consuming methods are solvothermal, precipitation, chemical precipitation, and hydrothermal. Most of the photocatalysts from the Table 2 are used for photodegradation of Methylene blue (MB), Rhodamine B (RhB) and Methyl orange (MO). In general, all methods represented in Table 2 produced photocatalyst with high efiiciency. However, some of them require the use of toxic precursor, like Na_2S, which in addition easily catches the water, or methods represented by the complexity of execution where it is necessary to maintain certain conditions, such as temperature, concentration or pH. For example, the use of Thioacetamine (TAA) as a source of sulfide ions, as in [47], is complicated due to the fact the process requires constant monitoring of the pH of the medium, since the rate of formation of sulfide ions decreases with a decrease in pH [48]. The approach presented in this study is represented by simplicity and environmental friendliness, and the photocatalysts with high efficiency can pre prapred in this way.

Table 2 – The photocatalytic experiments of CdS@ZnS nanostructures prepared with different approaches on the degradation of organic dyes

Synthetic method	Experimental conditions		Precursors	Light source	Dye	Photocatalytic efficiency	Rate constant (min^{-1})	[Ref]
	Time	T (°C)						
Solvothermal	10 h	180	$Zn(Ac)_2$, $CS(NH_2)_2$	-	Methylene blue (MB)	88.5%@12h	-	[49]
Ion adsoprtion	10 min	290	$Cd(Ac)_2 \cdot 2H_2O$, $Na_2S \cdot 9H_2O$, $Zn(Ac)_2 \cdot 2H_2O$	UV	Rhodamine B (RhB)	96.1%@35 min	0.0190	[50]
					MB	99.6%@35 min	0.0720	
Chemical precipitation	4 h	RT	$Cd(NO_3)_2$, H_2S, $ZnCl_2$	Vis	Acid blue (AB-29)	86.5%@90 min	0.0006	[51]
	9 h	80	$CdCl_2 \times 2H_2O$, $CS(NH_2)_2$, ZnS	UV	Congo red	98%	-	[52]
Solvothermal & Precipitation	24 h	170	$Cd(NO_3)_2 \times 4H_2O$, CS_2, $Zn(Ac)_2 \times 2H_2O$	UV	MO (Methyl orange)	77%@75 min	-	[47]
					Pyronin B (PyB)	66%@75 min	-	
					RhB	84%@75 min	-	
					MB	85%@75 min	-	
Hydrothermal	12 h	140	$CdCl_2 \times 5H2O$, $CS(NH_2)_2$, $Zn(Ac)_2$	Vis	MO	<95%@60 min	0.0625	[42]
Microwave-assisted	38 min	40	Pectin, NaOH, $Cd(Ac)_2$, TAA	Vis	RhB	98.7%@120 min	-	[17]
Two-step synthesis	3 h	180	$Cd(Ac)_2$, Na_2S, $Zn(Ac)_2$,	Vis	MO	<90%@90 min	0.0208	[44]
Sonochemical	40 min	RT	$Zn(Ac)_2$, TAA, CdS, NaOH,	UV	MB	42.6%@80 min	-	[53]
Mechanochemical	45 min	RT	$Cd(NO_3)_2$, $(NH_2)_2CS$, NaOH, $Zn(CH_3COO)_2$	Vis	Orange II	<99%@60 min	0.0516	this work

Hydrogen evolution by water splitting. Figure 8 displays the results of a photocatalytic experiment aimed to measure hydrogen evolution reaction (HER) using a photocatalyst. The experimental analysis involved monitoring the hydrogen release over a duration of 210 minutes. The obtained data reveals that the rate of hydrogen evolution when employing NiS-doped CdS/ZnS (45 min) photocatalyst exhibited an initial increase within the first 30 minutes, followed by a stabilization trend up to 180 minutes. The analysis indicates that the maximum rate of hydrogen evolution occurred at 19.3 μmolg^{-1}h^{-1} at the 120-minute mark. These findings suggest the existence of a synergistic effect and a direct correlation between the particle sizes of CdS and ZnS and their photocatalytic activity. These results imply that the high surface-to-volume ratio and the presence of defect sites at the photocatalyst interfaces play pivotal roles in enhancing the catalytic activity of nanostructured semiconductor composites. Additionally, the close interaction between CdS and ZnS particles emerges as a crucial factor contributing to enhanced photocatalytic activity [54]. Beyond the 180-minute mark, a decrease in hydrogen evolution is observed, attributed to the rapid recombination of electrons in the conduction band and holes in the valence band of CdS [55]. It is also noteworthy that ZnS exhibits limited absorption of visible light due to the excitation of certain defect states within the band gap [56]. These findings provide valuable insights for the design and optimization of photocatalytic systems for hydrogen production.

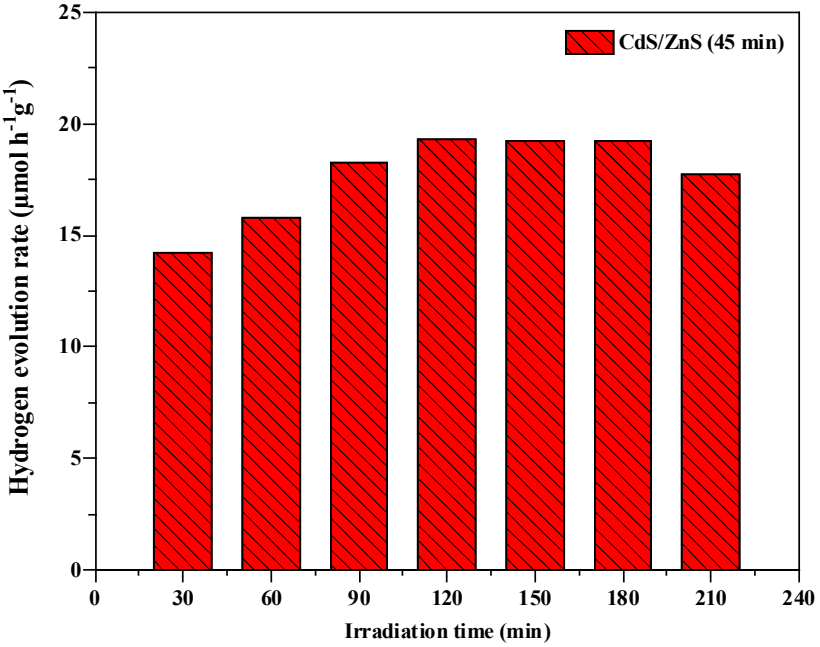

Figure 8 – Photocatalytic hydrogen generation performance of CdS/ZnS sample synthesized in 45 min

Conclusion

In this paper, a new facile solvent-free technology for the production of CdS@ZnS nanocomposites was demonstrated. This composite was obtained by partial substitution of Cd^{2+} ions by Zn^{2+} ions on the nanoparticles surface during mechanochemical reaction. The new solid-state method has several advantages: the method is environmentally friendly, economically beneficial and easily scalable. The fabricated CdS@ZnS nanocomposites have increased photocatalytic activity and are suitable for use in water purification from organic pollutans under the visible light irradiation. The scientific results of the conducted research open up the possibility of creating and producting the new doped metal sulfides nanocomposites for various purposes.

Acknowledgements

This research has been funded by the Committee of Science of the Ministry of Science and Higher Education of the Republic of Kazakhstan (Grant No. AP14870472). The support of Slovak Grant Agency VEGA (project 2/0112/22) is also gratefully acknowledged.

References

1. Schwarzenbach R. P., Egli T., Hofstetter T. B., Von Gunten U., Wehrli B. Global water pollution and human health // Annual review of environment and resources. – 2010. – T. 35. – C. 109-136.

2. Madhav S., Ahamad A., Singh A. K., Kushawaha J., Chauhan J. S., Sharma S., Singh P. Water pollutants: sources and impact on the environment and human health // Sensors in water pollutants monitoring: Role of material. – 2020. – C. 43-62.

3. Mishra S., Sundaram B. A review of the photocatalysis process used for wastewater treatment // Materials Today: Proceedings. – 2023.

4. Nemiwal M., Zhang T. C., Kumar D. Recent progress in g-C3N4, TiO2 and ZnO based photocatalysts for dye degradation: Strategies to improve photocatalytic activity // Science of the total environment. – 2021. – T. 767. – C. 144896.

5. Zhang F., Wang X., Liu H., Liu C., Wan Y., Long Y., Cai Z. Recent advances and applications of semiconductor photocatalytic technology // Applied Sciences. – 2019. – T. 9, № 12. – C. 2489.

6. Koe W. S., Lee J. W., Chong W. C., Pang Y. L., Sim L. C. An overview of photocatalytic degradation: photocatalysts, mechanisms, and development of photocatalytic membrane // Environmental Science and Pollution Research. – 2020. – T. 27. – C. 2522-2565.

7. Munyai S., Hintsho-Mbita N. Green derived metal sulphides as photocatalysts for waste water treatment. A review // Current Research in Green and Sustainable Chemistry. – 2021. – T. 4. – C. 100163.

8. Hajiyeva F., Ramazanov M., Shirinova H., Maharramova G. Photosensitive hybrid polymer nanocomposites on the base PVDF+ CdS/ZnS for solar cells application // Composite Interfaces. – 2022. – T. 29, № 3. – C. 236-254.

9. Chen Y., Xing W., Liu Y., Zhang X., Xie Y., Shen C., Liu J. G., Geng C., Xu S. Efficient and stable CdSe/CdS/ZnS quantum rods-in-matrix assembly for white LED application // Nanomaterials. – 2020. – T. 10, № 2. – C. 317.

10. Sağlam Ö., Dilgin Y. Fabrication of Photoelectrochemical Glucose Biosensor in Flow Injection Analysis System Using ZnS/CdS-Carbon Nanotube Nanocomposite Electrode // Electroanalysis. – 2017. – T. 29, № 5. – C. 1368-1376.

11. Murugadoss G., Kumar M. R. Optical and structural characterization of CdS/ZnS and CdS: Cu2+/ZnS core–shell nanoparticles // Luminescence. – 2014. – T. 29, № 6. – C. 663-668.

12. Chen L., Liu Y., Lai C., Berry R., Tam K. Aqueous synthesis and biostabilization of CdS@ ZnS quantum dots for bioimaging applications // Materials Research Express. – 2015. – T. 2, № 10. – C. 105401.

13. Fang D., Zhang Z., Wang Z., Ding Z. Study of photoluminescence of CdS/ZnS core/shell quantum dots // Physics Procedia. – 2012. – T. 32. – C. 920-925.

14. Hiemer J., Stöwe K. Continuous Flow Synthesis of Cd1-xZnxS and CdS/ZnS Core/Shell Semiconductor Nanoparticles by MicroJet Reactor Technology // ChemistryOpen. – 2022. – T. 11, № 12. – C. e202200232.

15. Bai L., Ge L., Gu J., Fang L., Li S. In situ synthesis of CdS/ZnS composite nanoparticles from ZIF-8 for visible light disposal of Cr (VI) // Journal of Sol-Gel Science and Technology. – 2021. – T. 99, № 1. – C. 211-219.

16. Huang M., Yu M., Si R., Zhao X., Chen S., Liu K., Pan X. Tailoring Morphology in Hydrothermally Synthesized CdS/ZnS Nanocomposites for Extraordinary Photocatalytic H2 Generation via Type-II Heterojunction // Catalysts. – 2023. – T. 13, № 7. – C. 1123.

17. Qin D., Yang G., Wang Y., Zhang J., Zhang L. Microwave-assisted synthesis of pectin-stabilised CdS/ZnS core/shell nanocrystals and enhanced photocatalytic performance // Micro & Nano Letters. – 2020. – T. 15, № 9. – C. 595-599.

18. Arab N., Fotouhi L., Salis A. Electrosynthesised CdS@ ZnS quantum dots decorated multi walled carbon nanotubes for analysis of propranolol in biological fluids and pharmaceutical samples // Microchemical Journal. – 2021. – T. 168. – C. 106453.

19. Wang X., Li X.-y. Heterostructure CdS/ZnS nanoparticles as a visible light-driven photocatalyst for hydrogen generation from water // International Journal of Green Energy. – 2016. – T. 13, № 12. – C. 1201-1208.

20. Bujňáková Z., Baláž M., Dutková E., Baláž P., Kello M., Mojžišová G., Mojžiš J., Vilková M.,

Imrich J., Psotka M. Mechanochemical approach for the capping of mixed core CdS/ZnS nanocrystals: elimination of cadmium toxicity // Journal of Colloid and Interface Science. – 2017. – T. 486. – C. 97-111.

21. Baláž P., Baláž M., Dutková E., Zorkovská A., Kováč J., Hronec P., Kováč Jr J., Čaplovičová M., Mojžiš J., Mojžišová G. CdS/ZnS nanocomposites: from mechanochemical synthesis to cytotoxicity issues // Materials Science and Engineering: C. – 2016. – T. 58. – C. 1016-1023.

22. James S. L., Friščić T. Mechanochemistry // Chemical Society Reviews. – 2013. – T. 42, № 18. – C. 7494-7496.

23. Friščić T., Mottillo C., Titi H. M. Mechanochemistry for synthesis // Angewandte Chemie. – 2020. – T. 132, № 3. – C. 1030-1041.

24. Baláž P., Achimovičová M., Baláž M., Billik P., Cherkezova-Zheleva Z., Criado J. M., Delogu F., Dutková E., Gaffet E., Gotor F. J. Hallmarks of mechanochemistry: from nanoparticles to technology // Chemical Society Reviews. – 2013. – T. 42, № 18. – C. 7571-7637.

25. Li X., Yu J., Low J., Fang Y., Xiao J., Chen X. Engineering heterogeneous semiconductors for solar water splitting // Journal of Materials Chemistry A. – 2015. – T. 3, № 6. – C. 2485-2534.

26. Shalabayev Z., Baláž M., Khan N., Nurlan Y., Augustyniak A., Daneu N., Tatykayev B., Dutková E., Burashev G., Casas-Luna M. Sustainable synthesis of cadmium sulfide, with applicability in photocatalysis, hydrogen production, and as an antibacterial agent, using two mechanochemical protocols // Nanomaterials. – 2022. – T. 12, № 8. – C. 1250.

27. Khan N., Baláž M., Burkitbayev M., Tatykayev B., Shalabayev Z., Nemkayeva R., Jumagaziyeva A., Niyazbayeva A., Rakhimbek I., Beldeubayev A. DMSO-mediated solvothermal synthesis of S/AgX (X= Cl, Br) microstructures and study of their photocatalytic and biological activity // Applied Surface Science. – 2022. – T. 601. – C. 154122.

28. Oskenbay A., Salikhov D., Rofman O., Rakhimbek I., Shalabayev Z., Khan N., Soltabayev B., Mentbayeva A., Baláž M., Tatykayev B. Solid-state synthesis of ZnS/ZnO nanocomposites and their decoration with NiS cocatalyst for photocatalytic hydrogen production // Ceramics International. – 2023. – T. 49, № 19. – C. 32246-32260.

29. Kumar S., Sharma J. Stable phase CdS nanoparticles for optoelectronics: a study on surface morphology, structural and optical characterization // Materials Science-Poland. – 2016. – T. 34, № 2. – C. 368-373.

30. Maleki M., Sasani Ghamsari M., Mirdamadi S., Ghasemzadeh R. A facile route for preparation of CdS nanoparticles // Semiconductor Physics Quantum Electronics & Optoelectronics. – 2007.

31. Chen Q., Bao H., Shen X. Phase transition of CdS in the presence of ethylenediamine and formation of hollow CdS submicron particles with needle-like structure // Phase Transitions. – 2008. – T. 81, № 6. – C. 591-601.

32. Pathak C., Mishra D., Agarwala V., Mandal M. Blue light emission from barium doped zinc sulfide nanoparticles // Ceramics International. – 2012. – T. 38, № 7. – C. 5497-5500.

33. Zhang J., Wang L., Liu X., Li X. a., Huang W. High-performance CdS–ZnS core–shell nanorod array photoelectrode for photoelectrochemical hydrogen generation // Journal of Materials Chemistry A. – 2015. – T. 3, № 2. – C. 535-541.

34. Tang Y., Liu X., Ma C., Zhou M., Huo P., Yu L., Pan J., Shi W., Yan Y. Enhanced photocatalytic degradation of tetracycline antibiotics by reduced graphene oxide–CdS/ZnS heterostructure photocatalysts // New Journal of Chemistry. – 2015. – T. 39, № 7. – C. 5150-5160.

35. Rossetti R., Nakahara S., Brus L. E. Quantum size effects in the redox potentials, resonance Raman spectra, and electronic spectra of CdS crystallites in aqueous solution // The Journal of Chemical Physics. – 1983. – T. 79, № 2. – C. 1086-1088.

36. Brafman O., Mitra S. Raman effect in wurtzite-and zinc-blende-type ZnS single crystals // Physical Review. – 1968. – T. 171, № 3. – C. 931.

37. Zahn D., Maierhofer C., Winter A., Reckzügel M., Srama R., Thomas A., Horn K., Richter W. The growth of cubic CdS on InP (110) studied in situ by Raman spectroscopy // Journal of Vacuum Science & Technology B: Microelectronics and Nanometer Structures Processing, Measurement, and Phenomena. – 1991. – T. 9, № 4. – C. 2206-2211.

38. Sivasubramanian V., Arora A., Premila M., Sundar C., Sastry V. Optical properties of CdS nanoparticles upon annealing // Physica E: Low-dimensional Systems and Nanostructures. – 2006. – T. 31, № 1. – C. 93-98.

39. Yu J., Li C., Liu S. Effect of PSS on morphology and optical properties of ZnO // Journal of colloid and interface science. – 2008. – T. 326, № 2. – C. 433-438.

40. Liu L.-w., Hu S.-y., Pan Y., Zhang J.-q., Feng Y.-s., Zhang X.-h. Optimizing the synthesis of CdS/ZnS core/shell semiconductor nanocrystals for bioimaging applications // Beilstein Journal of Nanotechnology. – 2014. – T. 5, № 1. – C. 919-926.

41. Weller H. Colloidal semiconductor q-particles: chemistry in the transition region between solid state and molecules // Angewandte Chemie International Edition in English. – 1993. – T. 32, № 1. – C. 41-53.

42. Xing R., Tong L., Liu X., Ren Y., Liu B., Ochiai T., Feng C., Chong R., Liu S. CdS/ZnS heterostructured porous composite with enhanced visible light photocatalysis // Journal of Nanoscience and Nanotechnology. – 2018. – T. 18, № 10. – C. 6913-6918.

43. Wang H.-J., Cao Y., Wu L.-L., Wu S.-S., Raza A., Liu N., Wang J.-Y., Miyazawa T. ZnS-based dual nano-semiconductors (ZnS/PbS, ZnS/CdS or ZnS/Ag2S,): A green synthesis route and photocatalytic comparison for removing organic dyes // Journal of environmental chemical engineering. – 2018. – T. 6, № 6. – C. 6771-6779.

44. Reddy C. V., Shim J., Cho M. Synthesis, structural, optical and photocatalytic properties of CdS/ZnS core/shell nanoparticles // Journal of Physics and Chemistry of Solids. – 2017. – T. 103. – C. 209-217.

45. Mestl G., Verbruggen N., Knözinger H. Mechanically activated MoO3. 2. Characterization of defect structures // Langmuir. – 1995. – T. 11, № 8. – C. 3035-3041.

46. Huang Z.-Q., Lu J.-P., Li X.-H., Tong Z.-F. Effect of mechanical activation on physico-chemical properties and structure of cassava starch // Carbohydrate polymers. – 2007. – T. 68, № 1. – C. 128-135.

47. Liu S., Li H., Yan L. Synthesis and photocatalytic activity of three-dimensional ZnS/CdS composites // Materials Research Bulletin. – 2013. – T. 48, № 9. – C. 3328-3334.

48. Monodispersed particles. / Sugimoto T.: Elsevier, 2019.

49. Wang L., Wei H., Fan Y., Liu X., Zhan J. Synthesis, optical properties, and photocatalytic activity of one-dimensional CdS@ ZnS core-shell nanocomposites // Nanoscale research letters. – 2009. – T. 4. – C. 558-564.

50. Zhang K., Jin L., Yang Y., Guo K., Hu F. Novel method of constructing CdS/ZnS heterojunction for high performance and stable photocatalytic activity // Journal of Photochemistry and Photobiology A: Chemistry. – 2019. – T. 380. – C. 111859.

51. Qutub N., Pirzada B. M., Umar K., Mehraj O., Muneer M., Sabir S. Synthesis, characterization and visible-light driven photocatalysis by differently structured CdS/ZnS sandwich and core–shell nanocomposites // Physica E: Low-Dimensional Systems and Nanostructures. – 2015. – T. 74. – C. 74-86.

52. Fakhri F. H., Ahmed L. M. Incorporation CdS with ZnS as composite and using in photo-decolorization of congo red dye // Indonesian Journal of Chemistry. – 2019. – T. 19, № 4. – C. 936-943.

53. Kaur G., Kaur A., Singh K. Study of Photocatalytic Activity of Synthesized Intrinsic and Extrinsic CdS/ZnS Core-shell Nanostructures //.

54. He J., Ji W., Mi J., Zheng Y., Ying J. Y. Three-photon absorption in water-soluble ZnS nanocrystals // Applied physics letters. – 2006. – T. 88, № 18.

55. Li Q., Guo B., Yu J., Ran J., Zhang B., Yan H., Gong J. R. Highly efficient visible-light-driven photocatalytic hydrogen production of CdS-cluster-decorated graphene nanosheets // Journal of the American Chemical Society. – 2011. – T. 133, № 28. – C. 10878-10884.

56. Xie Y. P., Yu Z. B., Liu G., Ma X. L., Cheng H.-M. CdS–mesoporous ZnS core–shell particles for efficient and stable photocatalytic hydrogen evolution under visible light // Energy & Environmental Science. – 2014. – T. 7, № 6. – C. 1895-1901.